International Journal of Precision Engineering and Manufacturing (2021) 22:1923–1936
https://doi.org/10.1007/s12541-021-00592-0

Online ISSN 2005-4602
Print ISSN 2234-7593

REGULAR PAPER

Influence of the Billet Volume Distribution on Macro Deformation and Microstructure Response in Transitional Region of Ti-Alloy Multi-rib Component Under Isothermal Local Loading

Ke Wei[1] · Qing Ma[1] · Haibing Tang[1] · Xiaoguang Fan[2] · Jian Zhang[2]

Received: 29 September 2020 / Revised: 24 May 2021 / Accepted: 28 September 2021 / Published online: 18 October 2021

Abstract
The folding, die underfilling, rib shifting and average grain size of primary equiaxed α were investigated using five different unequal thickness billets in transitional region of Ti-alloy multi-rib component under isothermal local loading and compared with integral loading. In terms of the macro deformation, the results show that the material transfers from the second-loading zone into the first-loading zone and the die underfilling decreases with the initial volume of the first-loading zone increasing, which reduces the risk of folding and rib shifting. However, that folding and rib shifting did not appear during the integral loading. Nevertheless, when the initial volume of the first-loading zone reaches a certain value, the die underfilling is aggravated both in local and integral loading. With respect to the microstructure, as the initial volume of the first-loading zone increases, the average grain size is decreased after the first-loading step, but increased after the second-loading step with consideration of one single loading step, which lead to the grain size being barely influenced by different billet volume distribution under both loading steps.

Keywords Isothermal local loading · Multi-rib component · Transitional region · Unequal-thickness billet

1 Introduction

Large-sized titanium alloy component with multi-rib features has been widely used in aviation and aerospace fields because of its high-performance and light-weight [1, 2] characteristics. However, in terms of the hard-to-form characteristic of the titanium alloy, irregular distribution of the inner rib and large projection area of the structure, a heavy-duty press with large tonnage and high stiffness is required to form such component by traditional forging technology, so as to meet the necessary load capacity. With the development of the airliner and new-generation fighter, the size of manufactured components will increase. Under the circumstance, the press capacity will be improved to keep up with the increased component size. To avoid that, it is necessary to develop a new technique for precise plastic forming that requires less-loading of the large-sized titanium alloy multi-rib components.

Isothermal forging can reduce the flow stress of the material because the workpiece can be formed without die chilling [3, 4]. The local loading forming is a flexible and force-saving method of changing the loading zones [5, 6], in which a load is exerted to a part of the billet and finally the integral component can be formed, as shown in Fig. 1. By combining the advantages of isothermal forging and local loading, the isothermal local loading forming (ILLF) is a precise forming technology requires a less-loading [7], which provides an efficient method to manufacture large-sized titanium alloy multi-rib components.

In the ILLF, the transitional region determines the performance of the integral large-sized component. Particularly, the alternation between the loading zone and unloading zone can result in reciprocating flow of material in the transitional region [8]. This specific characteristic of the ILLF

✉ Ke Wei
weike@nchu.edu.cn

✉ Xiaoguang Fan
fxg3200@nwpu.edu.cn

[1] National Defense Key Discipline Laboratory of Light Alloy Processing Science and Technology, School of Aeronautical Manufacturing Engineering, Nanchang Hangkong University, Nanchang 330063, China

[2] State Key Laboratory of Solidification Processing, School of Materials Science and Engineering, Northwestern Polytechnical University, Xi'an 710072, China

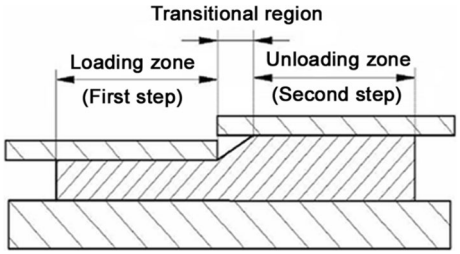

Fig. 1 Illustration of the local loading forming [5]

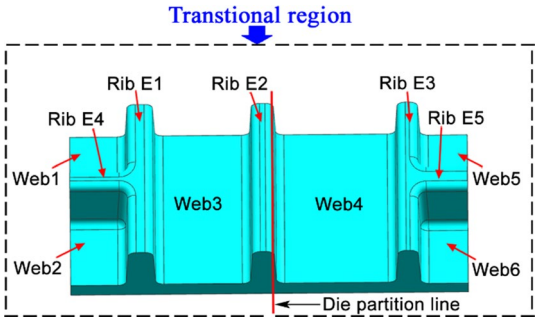

Fig. 2 Eigenstructure representing the transitional region in local loading

process is called as material transfer here. The transferred material in the second-loading zone may lead to folding [9], die underfilling [10] and rib shifting [11]. The complicated material transfer will intensify the inhomogeneous deformation, which makes the microstructure in transitional region hard to control [12]. Therefore, the material transfer plays a crucial role in the micro and macro forming quality of the transitional region in ILLF of the large-sized titanium alloy multi-rib component. So, it is important to reveal the macro deformation and microstructure response in transitional region under the ILLF process.

Previous work has been done on deformation analysis in the transitional region of the ILLF for titanium alloy components. Sun et al. [7] suggested a proper positioning of the die partitioning boundary along the rib that is helpful for the transferred material filling in the cavity of that rib. Gao et al. [9] revealed that decreasing the spacer block thickness and increasing the friction are beneficial to decrease the quantity of transferred material, which can reduce the risk of folding. Besides, increasing the fillet radii of the partitioning rib in the transitional region can also reduce the risk of the folding. Concerning the microstructure response, Li et al. [13] pointed out that increasing the width of the adjacent rib in the transition region result in increased concavity of the cross ribs and a decrease in the average grain size. Moreover, with a decrease in forging temperature and an increase in loading speed, there is a decrease in the average grain size. In the referenced works, all the investigations are relative to the transitional region, providing good guidance for improving the forming ability of the transitional region. Nevertheless, during the bulk forming process, the billet volume distribution largely determines the material flow of the cavity-filling of the die [14, 15], especially for problems with reciprocating flow of the material under the conditions of multi-step local loading process. Therefore, further investigation is required to evaluate the influence of billet volume distribution on macro deformation and microstructure response in the transitional region of titanium alloy multi-rib component under ILLF.

The purpose of this work is to study the macro deformation and microstructure response with consideration of the influence of the billet volume distribution in transitional region under the ILLF process. Firstly, a 3D finite element (FE) model of a multi-rib eigenstructure was established to represent the transitional region of the local loading forming. Then, the FE model was verified by physical experiments of macroscopic deformation and microstructure. Subsequently, the geometric parameters of the billet for distributing the initial volume in transitional region were described. Finally, the influence of the billet volume distribution on folding, die underfilling, rib shifting as well as the average grain size of primary equiaxed α were identified using five different UTBs based on FE simulation. This knowledge provides guidelines for macro deformation and microstructure control of ILLF for large-sized titanium alloy component with multi-rib features.

2 FE Modelling and Verification

2.1 Eigenstructure of the Multi-Rib Component in the Transitional Region

According to the local loading feature of the full-size multi-rib component, the impact of a loading zone on an unloaded zone is a short range effect [16, 17], which affects the region from die partitioning line to its adjacent rib of unloading region. Therefore, the influence of local loading feature on the full-size component is among the three adjacent ribs when the die partitioning line is located on the second one. In the full-size component, the region near these three ribs is called transitional region. Thus, due to the structural features of the multi-rib component, an eigenstructure which includes three transverse ribs and two longitudinal ribs is extracted to represent the transitional region of the ILLF, as shown in Fig. 2. The whole eigenstructure is the transitional region which can reflect the detailed forming characteristics so as to investigate the macro deformation and microstructure response in transitional region of full-size multi-rib component under ILLF. In addition, based on the deformation analysis of the eigenstructure, detailed forming

characteristics of the transitional region can be observed and the FE simulation time can be significantly reduced based on this eigenstructure rather than the full-size component, since this work is focus on the transitional region of the ILLF. To reflect the asymmetric and complex characteristic of the rib-web component, the thicknesses of some webs, the distances between each rib and width of the ribs are varied. The geometric parameters and sizes of the eigenstructure are given in Table 1.

2.2 FE Modelling

Nowadays, FE simulation is an essential stage during the analysis of the material forming process because it can provide various forming information such as the material flow, the evolution of the defects and the changing process of the grain size [18–21]. Thus, the FE simulations under a DEFORM-3D environment were carried out in this work. Due to symmetry in the center of ribs 4 and 5 of the eigenstructure, the 1/2 structure was selected to improve calculating efficiency, thus reduced the simulation time. Then, the FE model of the transitional region was established, as shown in Fig. 3a, b. It can be seen from Fig. 3a that the local loading on the workpiece is achieved by adjusting the relative position of two bottom dies using a spacer block. Firstly, the local zone of the workpiece above the spacer block can be formed during the first-loading step. Then, the exerted force transfers to the other zone of the workpiece during the second-loading step, in which the spacer block is removed and two subparts of the bottom die are coplanar. During the local loading process, the reduction amount of each loading step is 14 mm, the accumulative reduction amount of two

Table 1 Geometric parameters and sizes of the eigenstructure

Feature	Parameter	Value	Feature	Parameter	Value
Rib E1	Width, W_1 (mm)	15	Web 1	Thickness, T_1 (mm)	13
	Height, H_1 (mm)	44	Web 2	Thickness, T_2 (mm)	13
Rib E2	Width, W_2 (mm)	13	Web 3	Thickness, T_3 (mm)	14
	Height, H_2 (mm)	43	Web 4	Thickness, T_4 (mm)	14
Rib E3	Width, W_3 (mm)	12	Web 5	Thickness, T_5 (mm)	12
	Height, H_3 (mm)	45	Web 6	Thickness, T_6 (mm)	12
Rib E4	Width, W_4 (mm)	12	Distance	To the left side of rib 1, D_{01} (mm)	35
	Height, H_4 (mm)	44		Between ribs 1 and 2, D_{12} (mm)	60
Rib E5	Width, W_5 (mm)	16		Between ribs 2 and 3, D_{23} (mm)	75
	Height, H_5 (mm)	45		To the right side of rib 3, D_{30} (mm)	30

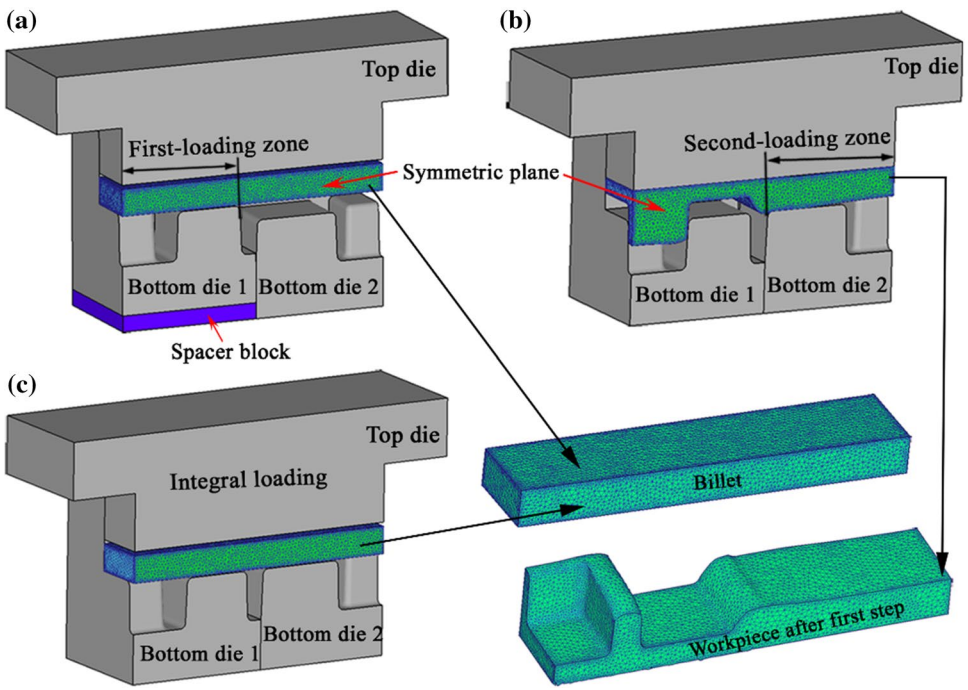

Fig. 3 FE model of eigenstructure: the first-loading step (**a**) and the second-loading step (**b**) of the local loading; **c** the integral loading

steps is thus 28 mm. In reference to the result by Gao et al. [22], a desirable thickness for the spacer block (14 mm) was chosen in this work.

The ILLF process is performed under high temperature (970 °C) and relatively low speed (0.2 mm/s), and the thermal events are ignored in FE model. The Mises yielding criteria and the isotropic hardening rule are adopted. The shear friction model is employed to describe the friction behavior between the dies and workpiece. The friction factor is determined to be 0.5 in this work, according to the friction experiment from Zhang et al. [23]. To meet the simulation requirement of the severe plastic deformation, the tetrahedral solid element was adopted and the total number of meshed elements for the billet is 80,000. Besides, the local mesh refinement of the plastic deformation zone and mesh automatic redivision were carried out. For better understand on the macroscopic deformation and microstructure evolution during the local loading process, the FE model of the integral loading forming is also established, as shown in Fig. 3c.

Additionally, the combined dies are considered as rigid bodies due to their stiffness, the elastic deformation of the workpiece was neglected in this work since its plastic deformation is much larger. Besides, the body force of the workpiece was also ignored. Therefore, the billet is regarded as rigid-plastic type, whose material is TA15 titanium alloy in FE modeling. Similarly, TA15 was also considered as rigid-plastic material rather than elastic–plastic material in the work of Fan et al. [2]. The material model is input into the FE simulation software by the form of discrete points based on the work of Shen [24], as the stress–strain relations shown in Fig. 4. The deformation temperature of the workpiece is 970 °C in the present study and the constitutive curve of the current temperature can be acquired by automatic interpolation in FE simulation software.

The internal state variable (ISV) material model was established based on the softening mechanism of material deformation and the microstructure evolution law [25], which can be adequately used in predicting the microstructure evolution during a hot forming process. Therefore, in this work, a set of equations describing microstructure evolution of the TA15 titanium alloy were developed based on the ISV method, which take the following form [26]:

$$\begin{cases} \dot{\rho} = k_1\sqrt{\rho}\,\dot{\varepsilon} - \left(k_2\rho\,\dot{\varepsilon}^{m} k_3\rho^{n}\right)\exp(-Q_s/RT) - k_4\rho\dot{S}\Big/(1-S) \\ \dot{d} = \alpha_1 d^{-\gamma_1} - \alpha_2\,\dot{S}^{\gamma_3}\,d^{\gamma_2} \\ \dot{S} = \beta_1\gamma\rho\exp\left(-Q_b/RT\right)/d \\ \rho_{cr} = \beta_2\left[\dot{\varepsilon}\exp\left(Q_z/RT\right)\right]^{\lambda_1} \\ \gamma = (0.1+S)^{q}(1-S)\rho/\rho_{cr} \end{cases} \tag{1}$$

where $\dot{\rho}$, $\dot{d}$, $\dot{S}$ are the dislocation density, the average grain size of primary equiaxed α and recrystallization volume fraction, respectively. $k_1 \sim k_4$, α_1, α_2, $\gamma_1 \sim \gamma_3$, β_1, β_2, λ_1, m, n, q, Q_s, Q_b, Q_z are the material constant. R is the gas constant, which is taken as 8.13145 J/(mol K).

The material constants were calculated by Han et al. [26], as shown in Table 2. The accuracy of the ISV model has been tested which can meet the needs of the application requirement. Subsequently, the ISV material model of TA15 titanium alloy was encoded into the DEFORM-3D platform by the FORTRAN language.

2.3 FE Model Validation

Robinson et al. [27] pointed out that the physical simulation experiment (PSE) using a softer material provides distinct

Table 2 Material constants for ISV material model [26]

Material constant	Value	Material constant	Value	Material constant	Value
k_1	385.46	γ_1	19.59	m	0.68
k_2	$2.51e^{6}$	γ_2	0.67	n	2.85
k_3	$2.38e^{4}$	γ_3	1.11	q	$1.52e^{-4}$
k_4	69.86	β_1	$2.76e^{7}$	Q_s	$1.08e^{5}$
α_1	$5.83e^{-3}$	β_2	$3.83e^{-2}$	Q_b	$2.04e^{5}$
α_2	1.54	λ_1	$3.86e^{-2}$	Q_z	$5.78e^{5}$

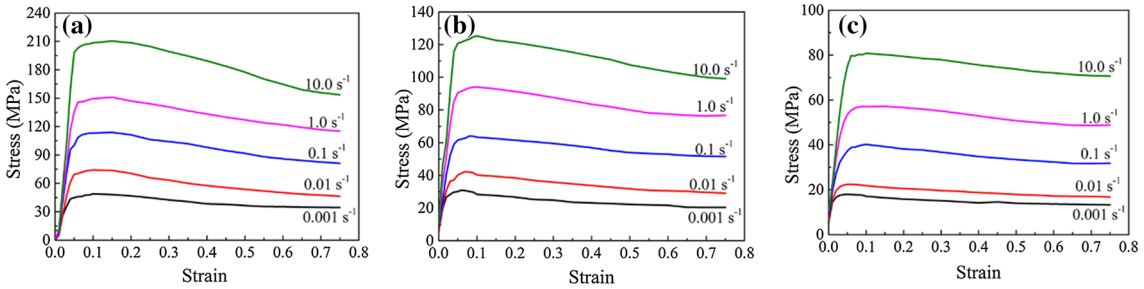

Fig. 4 Stress–strain curves of TA15 under different temperatures [24]: **a** 900 °C; **b** 950 °C; **c** 1000 °C

advantages for metal forming research, such as the cost savings, easy operating and environment protection. Therefore, the FE model has been validated by PSE with lead in this work. The PSE was conducted at room temperature instead of the titanium alloy at high temperature [28]. Dies and equal-thickness billet (ETB) for the physical experiment are shown in Fig. 5 and the material of die was 5CrNiMo steel. Consistent grease was used for lubricating the dies and workpiece. The key forming results of the PSE and FE simulation are listed in Table 3. Among them, H_{left}, H_{middle} and H_{right} represent the height of the rib 1, rib 2 and rib 3 on the symmetric plane by local and integral loading, while D_{fold} represents the distance between the folding and the center of rib 2 by local loading, as shown in Fig. 6. Good agreement on four key sizes between the PSE and simulated workpiece indicate that the FE model was reliable in studying the macroscopic deformation in the transitional region of local loading forming.

Furthermore, in order to validate the reliability of the FE model for the microstructure development of the ILLF, the

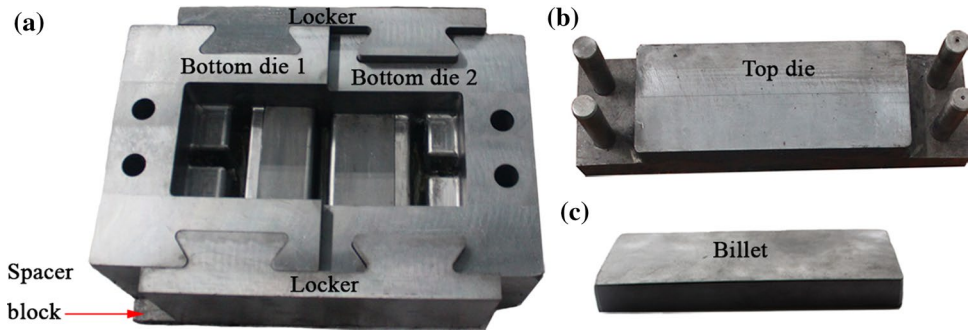

Fig. 5 Dies and billet for physical experiment [10]: **a** assemble bottom die; **b** top die; **c** equal-thicknessbillet

Table 3 Comparison of forming results between FE simulation and experiment [10]

	Local loading				Integral loading		
	H_{left} (mm)	H_{middle} (mm)	H_{right} (mm)	D_{fold}(mm)	H_{left} (mm)	H_{middle} (mm)	H_{right} (mm)
Experiment	38.7	42.9	40.0	30.5	42.1	42.9	42.7
FE simulation	41.4	43.0	43.0	27.8	43.0	43.0	43.0
Relatively error (%)	6.52	0.23	6.98	8.85	2.09	0.23	0.70

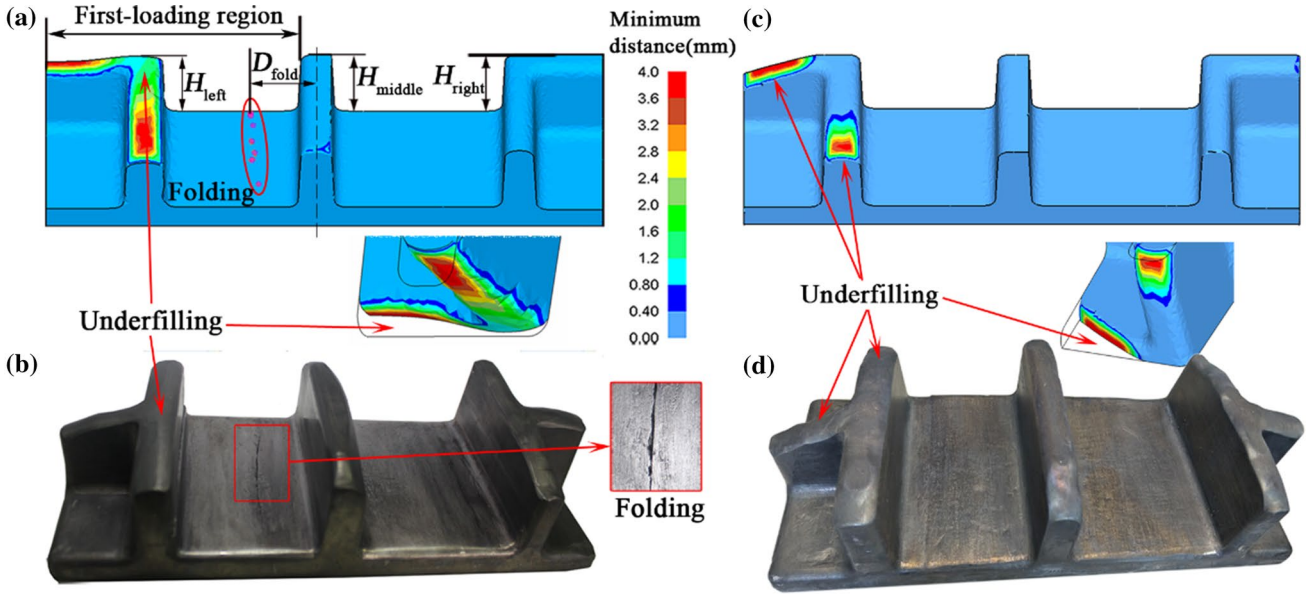

Fig. 6 Simulated result (**a**) and experimental result (**b**) of the local loading [10]; simulated result (**c**) and experimental result (**d**) of the integral loading

experiment of the local loading with an isothermal condition was carried out by Han et al. [26]. During the experiment, the forming temperature was 950 °C and the loading speed of top die was 1 mm/s. After two loading steps, the microstructure morphology of the different loading zones can be observed in literature [26]. The comparison of the experimental results and FE simulation is given in Table 4. It was found that the FE model predictions are very close to the experiment. Therefore, Eq. (1) indicated a good prediction in the FE simulation on the microstructure response during the ILLF process.

3 Geometric Parameters Description of the Billet Volume Distribution

The billet volume distribution was adjusted by the unequal-thickness billet (UTB), which is simple and convenient to manufacture, as shown in Fig. 7a. For better implementation of the reasonable initial volume distribution under the principle of constant volume, the UTB was divided into three parts rather than two parts. According to the research by Zhang et al. [29], it was better to adopt a beveling type in variable-thickness regions of the UTB, so as to meet the requirements of easy manufacturing and to reduce the possibility of folding in that region, as shown by the shaded area in Fig. 7a. The quantitative index of the beveling can be defined as:

$$R_b = \Delta l / \Delta H \tag{2}$$

where Δl and ΔH are the lengths of beveling and thickness differences of adjoining parts. According to the recommended value by literature [29], the value 2 is suggested for R_b.

It can be seen from Fig. 7a that the initial volume of the UTB can be effectively distributed by five size parameters: H_1, H_2, H_3, l_{left} and l_{right}. To realize the volume difference of the billet in different loading zone under the constant-volume principle, H_1 is defined as an independent variable, while H_3 is defined as a dependent variable. The rest are fixed values. The value of H_1 is changed based on UG softeware, then five UTBs with different volume percentages (Exp-1 to Exp-5) were designed for arranging the single factorial experiments. The detailed size parameters are listed in Table 5 and five volume percentages of the UTBs (Exp-1 to Exp-5) are shown in Fig. 7b. In summary, as H_1 increased, the initial distributed volume in the first-loading zone also increased. Therefore, the initial volume distribution in the transitional region can be actively adjusted and controlled by the size of H_1. Subsequently, a parametric study was carried out via numerical simulation to investigate the effects of billet volume distribution on macro deformation and

Table 4 Comparison of average grain size of primary equiaxial α [26]

	Experiment	Simulation
First-loading zone	7.86 μm	7.38 μm
Second-loading zone	7.45 μm	7.29 μm

Table 5 Variable and fixed values for geometric parameters of UTB under single-factor experiment

Variable	Exp-1	Exp-2	Exp-3	Exp-4	Exp-5
H_1 / H_e	0.75	0.85	0.95	1.05	1.15
Volume percentage under the first-loading step (%)	38.11	40.80	43.69	46.77	50.05
H_2/H_e	1	1	1	1	1
l_{left}/l_{left}	0.6	0.6	0.6	0.6	0.6
l_{right}/L_{right}	0.6	0.6	0.6	0.6	0.6

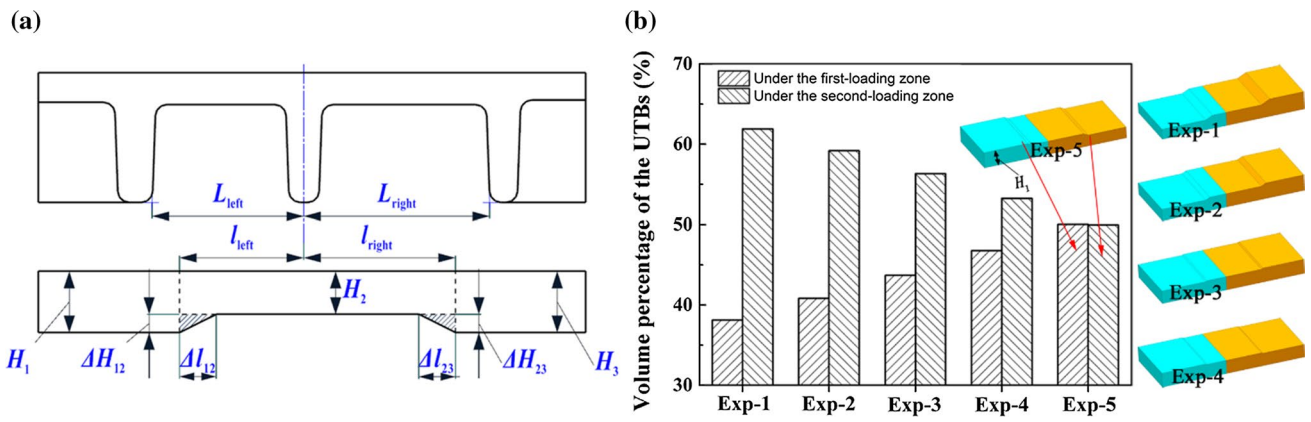

Fig. 7 Geometric parameters description of the UTB: **a** the section of the UTB; **b** billet volume distribution in the different loading zones of the transitional region

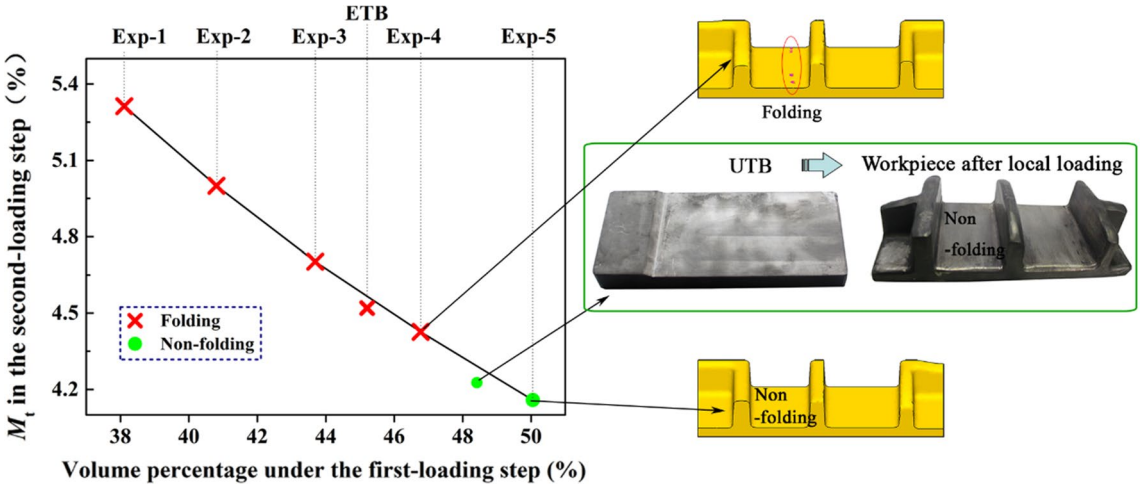

Fig. 8 Influence of the different volume distributions of the billet on M_t and folding in the second-loading step of the transitional region

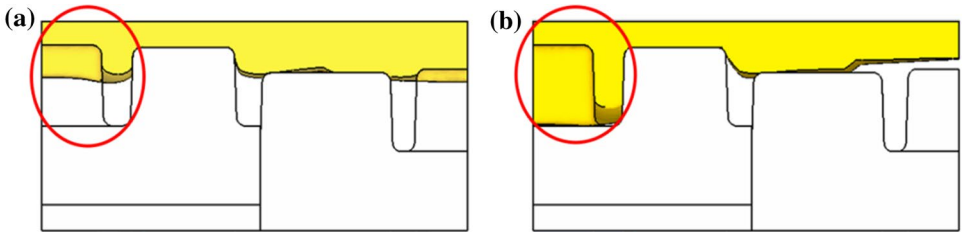

Fig. 9 The workpieces after the first-loading step by the billets of Exp-1 (**a**) and Exp-5 (**b**)

microstructure response in transitional region of Ti-alloy multi-rib component under ILLF.

4 Results and Discussion

4.1 Material Transfer and Folding

In previous studies [9, 10], the results showed that the folding defect is prone to emerge in the transitional region during local loading of the multi-rib component. Figure 8 illustrates the variation of material transfer by five different UTBs. It can be seen that M_t (M_t represents the percentage of transferred material) decreased with an increasing initial volume of the first-loading zone. The explanation of this phenomenon is that the filling depth of the cavity of the rib in the first-loading zone is increased with an increase in the distributed initial volume in the first-loading zone. Accordingly, the distributed initial volume in the second-loading zone is relatively less, due to the constant-volume principle. Then, the quantity of the transferred material in the second-loading zone was decreased. Figure 9 compared the filling depth of the rib by Exp-1 and Exp-5 after the first-loading step. It is clearly to see that the formed height of the rib by Exp-5 is higher than that of Exp-1. Meanwhile, the material in the second-loading zone by Exp-5 is less than Exp-1.

Table 6 Folding situations by the physical simulation experimental samples

Experimental samples	Volume percentage under the first-loading step (%)	M_t	Folding generation by FEM	Folding generation by experiment
ETB	45.21	4.55	Yes	Yes
UTB	48.42	4.21	No	No

It can be seen in Fig. 8 that folding is generated by Exp-1 to Exp-4, while folding was avoided by Exp-5. The detailed evolution process of that folding was observed and discussed in our previous work [10]. It can be concluded that there exists a critical value of M_t. When the transferred material exceeds that critical value, folding might occur. How to acquire the critical value is detailed in Ref. [10]. To verify that increasing the billet volume of the first-loading zone is favorable to eliminate folding, a physical simulation experiment of UTB was carried out, in which the billet volume of the first-loading zone was more than ETB's. The folding results of the experiment and FE simulation by ETB and UTB are summarized in Table 6. The results show that non-folding was observed in the experimental results of UTB, as shown in Fig. 8, while folding was generated by the ETB outcomes, as shown in Fig. 6b. Therefore, it can

be concluded that increasing the billet volume of the first-loading zone can decrease the transferred material, which is beneficial to reduce the risk of folding.

4.2 Die Filling

The previous research showed that the material could flow into all the die cavities of the ribs in the transitional region during the second-loading step [10], thus the die filling of the first-loading zone after first-loading step can be changed during the second-loading step. Therefore, the analysis of die filling was only focused on the second-loading step. To quantitatively analyze the die filling behavior in transitional region by the billet volume distribution, the die underfilling rate Φ_u was adopted to depict the cavity-filling capacity of the rib, which takes the form:

$$\Phi_u = \left(V_{\text{underfill}}/V_{\text{eigen}}\right) \times 100\% \tag{3}$$

where $V_{\text{underfill}}$ is the underfilled volume of the eigenstructure when a certain rib (rib E1 and E4, rib E2 or rib E3 and E5) is fully filled before any other ribs during the second-loading step. Following this rule, as Φ_u approaches zero, better die filling can be acquired.

Figure 10a illustrates the influence of the rule on cavity-filling of the rib under different billet volume distributions. It can be seen that the die underfilling rate Φ_u by two local loading steps decreases first, then increases with the billet volume distribution of the first-loading zone increasing. As the minimum distance shown in Fig. 10b, the cavity-filling of the rib in the first-loading zone or in the second-loading zone was fully filled. The reason is that the cavity-filling of the rib in the second-loading zone can be fully filled beforehand by Exp-1 to Exp-4, so as more billet volume is distributed in the first-loading zone, cavity-filling of the rib in transitional region will improve. However, when the billet volume of the first-loading zone reaches a certain value, the cavity-filling of the rib in the first-loading zone can be fully filled beforehand, as the Exp-5 shown in Fig. 10b. Hence, the die underfilling was aggravated in the second-loading zone and consequently the cavity-filling of the rib in the transitional region became worse compared to Exp-4 and Exp-5. It should be noted that the die underfilling of Exp-3 and Exp-5 was almost the same. Although the similarity of the die filling in the transitional region can be acquired by different billet volume distributions, Φ_u is the index of the quantitative analysis for the die filling behavior, which means that the material flows into the various cavities of the rib owing to the feature of the multi-rib component. If one cavity-filling of the rib becomes better, this may lead to the other cavity-filling of the rib becoming worse. In this work, one of the aims was to determine the effect of the billet volume distribution on die filling in transitional region of ILLF, so as to optimize that billet for balance and acquire the optimum die filling. So the influence of the different volume distribution of the billet on Φ_u and similar results for the cavity-filling of the rib under different billet volume distribution are reasonable in this work.

To analyze the effect of transferred material on the cavity-filling of the rib, the die underfilling rate Φ_u by integral loading is given as a comparison in Fig. 10a and c. The result shows that there exists a certain discrepancy between integral loading and local loading, but the variation trend of the die underfilling rate Φ_u is the same in either case.

From the analysis above, the transferred material may have an effect on die filling in the transitional region. To further study the effect of transferred material on die filling during the second-loading step, the quantitative analysis of the volume percentage variation within the first-loading zone is given in Fig. 11a. The results show that all the UTBs exhibit

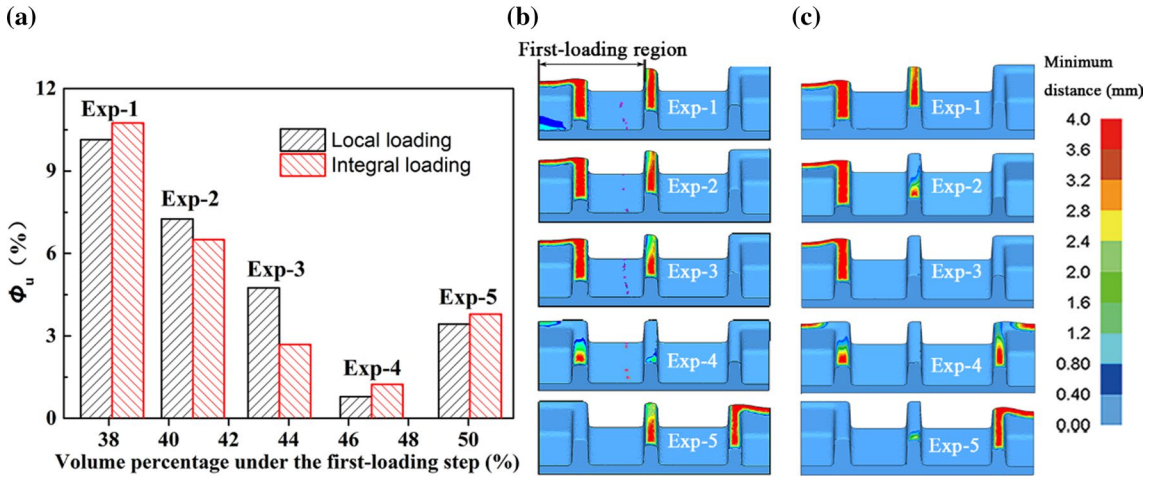

Fig. 10 Influence of the different volume distributions of the billet on Φ_u: **a** the variation tendency of Φ_u; **b** local loading; **c** integral loading

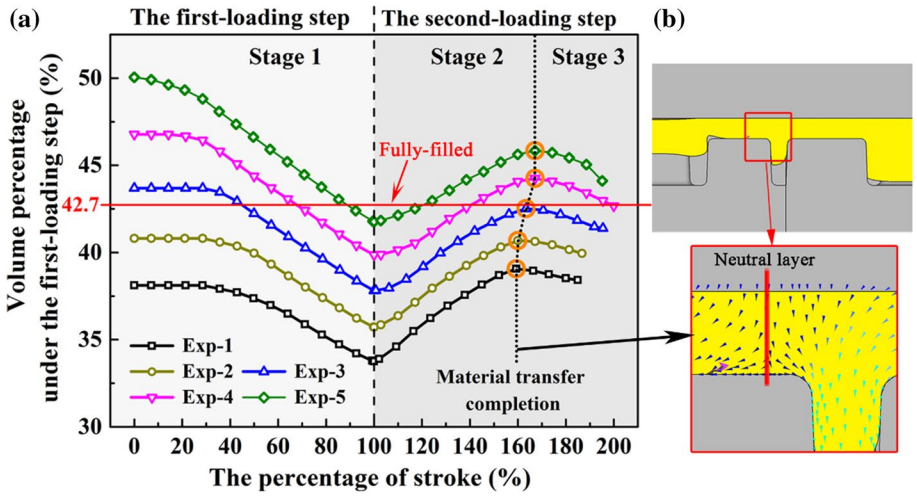

Fig. 11 Illustration of the variation of the volume during the first-loading zone: **a** variation of the volume with the top die descending; **b** formation of the neutral layer during the second-loading step

the same tendency. Besides, the material variance in the first-loading zone can be divided into three stages according to the material transfer pattern. In stage 1, the material variance under the first-loading zone is a continuous declination throughout the first-loading step since the top die presses the billet. The reason is that the material in the first-loading zone is not constrained by the other subpart of the die, which is located in the unloading zone. Consequently, the initial distributed material in the first-loading zone was transferred into the second-loading zone continuously, leads to decrease of material in the first-loading zone during the first stage. The second stage starts from the beginning of the second-loading step. The material in the second-loading zone was transferred into the first-loading zone, leading to an increase of material in the first-loading zone during the second stage. With the top die descending, a neutral layer is formed when the second stage finished, as shown by the red vertical line in Fig. 11b. At this moment, the material in the second-loading zone no longer transferred into the first-loading zone. In stage 3, the material in the first-loading zone flowed along both sides of the neutral layer. One part of the material flowed into the cavity-filling of the rib in first-loading zone. The other part of the material turned toward the second-loading zone and flowed into the partitioning rib, which was the main reason for decreasing material in the first-loading zone during the third stage.

Notably, there is a transverse red line between 40 and 45% of the volume percentage under the first-loading step in Fig. 11a, which means the target die filling of the first-loading zone is 42.7%. So the cavity-filling of the die under the first-loading zone is fully-filled at 42.7% after two local loading steps. Therefore, Fig. 11 can further reveals that Exp-4 has lowest die underfill and Exp-1 has highest die underfill among Exp-1 to Exp-5.

By scrutinizing the results in Figs. 10 and 11, the root cause of the difference on cavity-filling of the rib between the local loading and integral loading was the reciprocating material transfer during the first and second-loading step. Although the quantity of transferred material in the first and second loading steps are inequality, the variation tendency of the cavity-filling of the rib by local loading and integral loading are the same, indicating that the material transfer has little influence on die filling. The cavity-filling of the rib in the transitional region is essentially dependent on initial volume distribution.

4.3 Rib Shift

In our previous analysis on the rib shift of local loading, the affected zone of rib shift is near the root of the formed rib on the first-loading zone side in transitional region [11]. Therefore, the changing displacement of point D1 in Fig. 12 was chosen as the research object for rib shifting analysis by different billet volume distribution. It can be seen that

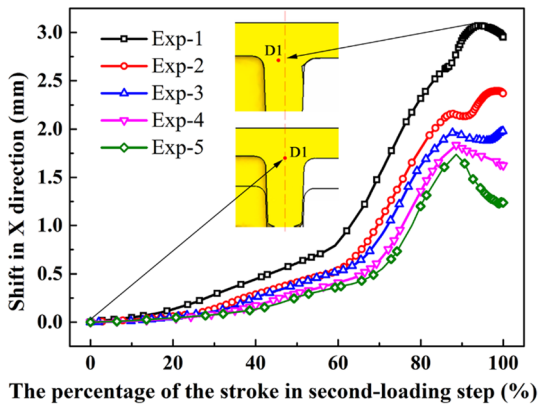

Fig. 12 Changing displacement of point D1 in X direction during the second-loading step under the different billet volume distributions in transitional region

the offset of D1 in the X direction decreased with the billet volume of the first-loading zone increasing, i.e. the degree of the rib shifting decreased. The reason is that the transferred material during the second-loading step decreased with the initial volume of the billet in first-loading zone increasing. Subsequently, the compressive stress (caused by the transferred material), which exerts on the rib shift can also be decreased. The conclusion can be drawn that a decreased initial volume of the billet in the second-loading zone is an effective method to relieve the rib shifting during the local loading process. Moreover, rib shifting as well as folding did not appear during the integral loading.

4.4 Grain Size

Different strain paths under local loading and integral loading may bring about a diverse microstructure. In order to reflect the strain and grain size in the transitional region, a simple ETB was adopted to observe its distribution on the workpiece after one and two local loading steps, as shown in Fig. 13a and b. Additionally, the strain distribution of the formed workpiece by the integral forming is depicted as a comparison in Fig. 13c. The accumulated strain by two steps of local loading results in a distinct strain concentration, and the corresponding zone within this strain concentration is called the affected zone, which is not observed after the integral forming.

Based on the established ISV model, the grain size distribution after the first and second-loading steps are shown in Fig. 13d and e. Meanwhile, the grain size distribution by the integral loading is also given as a comparison, as shown in Fig. 13f. It can be seen from the affected zone by local loading features that the grain size is smaller compared to the integral loading. It is well known that the microstructural morphology varies with strain: the larger the strain, the smaller the grain size of the microstructure. Therefore, the variation of grain size is governed by two reasons:

(1) First, the transferred material would contact the top and bottom die 1 at the same time during the second-loading step. Then, the deformation is generated in the first-loading zone (unloading zone). Accordingly, the strain would be accumulated in the web that connects the partitioning rib to its adjacent rib in the unloading zone. However, that strain is not produced during the integral loading process due to nonoccurrence of the material transfer.
(2) Second, the deformation can be generated at the root of the rib in the first-loading zone (unloading zone) due to the rib shifting. Similar to the first reason, that strain is not produced during the integral loading process due to nonoccurrence of the rib shifting.

Moreover, the grain size distribution out of the affected zone is basically the same via the local loading and integral loading. Based on the common causes of the two reasons given above, in the transitional region of ILLF, the grain size distribution by the local loading is distinguished from that of integral loading, and the distribution area that is different is only in the affected zone.

Figure 14 compares the distribution of the grain size in the affected zone by a percentage. The results show that grain sizes less than 7 μm reached 89.3% under local loading, while grain sizes less than 7 μm was only up to 60.8%

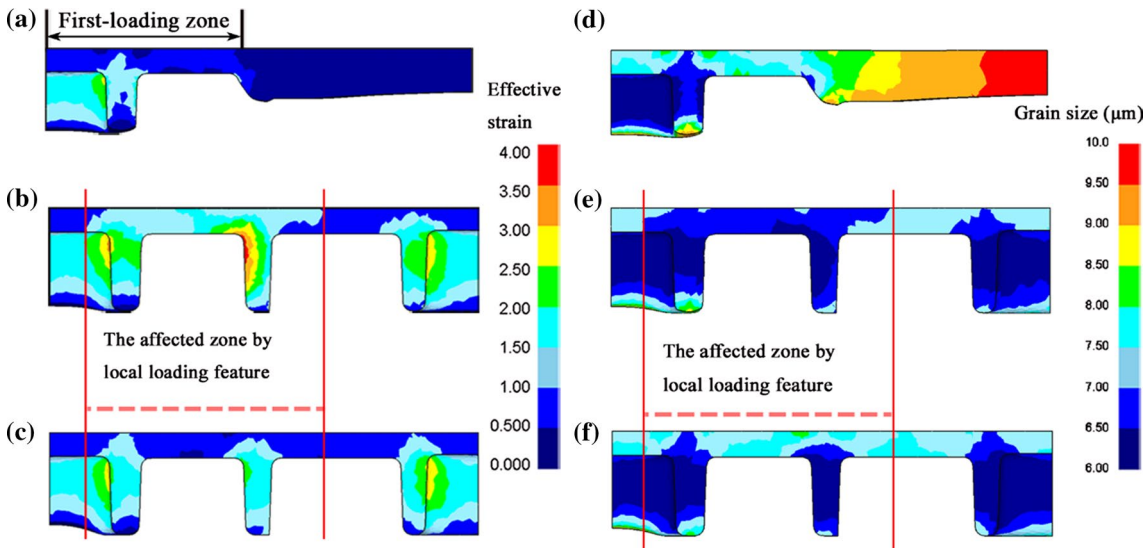

Fig. 13 Strain distribution after the first **a** and second **b** loading step of the local loading; **c** strain distribution after the integral loading [11]; Grain size after the first **d**, second **e** loading step of the local loading; **f** grain size after the integral loading

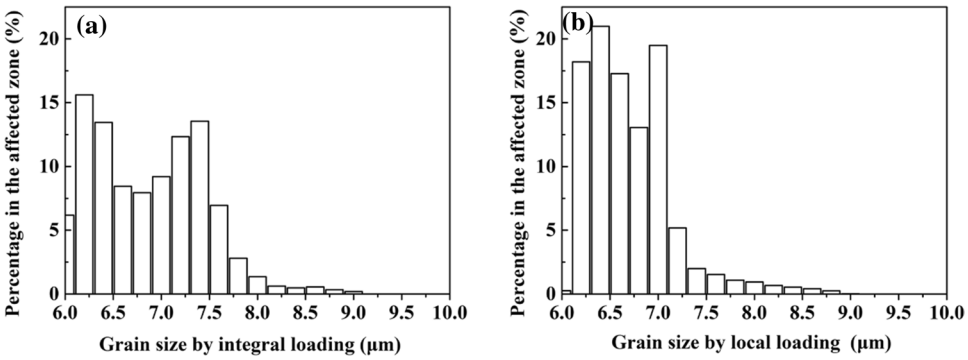

Fig. 14 Percentage distribution of the grain size in affected zone: **a** integral loading; **b** local loading

under integral loading. Therefore, the grain size under local loading is smaller on the whole compared with the grain size under integral loading, as shown in Fig. 15a. The statistics of the percentage distribution further reveals the grain size after local loading is significantly less than that after integral loading.

Figure 15a illustrates the influence of the billet volume distribution on the average grain size. After two local loading steps, the average grain size increased first and then decreased. But it is worth noting that the average grain size of Exp-1 to Exp-5 formed by the local loading varied from 6.6 to 6.7 microns. Generally speaking, this variance in average grain size is too small to justify the billet volume distribution affects the grain size. However, the strain was accumulated by the first and second loading steps, then the variation of the grain size inevitably took place during the single first and single second loading step. Therefore, further investigation is required to clarify the effect of the grain size in each single loading step.

Figure 15b illustrates the variation of the average grain size by a single loading step of the local loading under different billet volume distribution. It is observable that the average grain size after the first-loading step decreased with an increasing the initial volume in first-loading zone. On the contrary, that grain size after the second-loading step increased. This occurred because increasing the initial volume of the first-loading zone can lead to more material flow into the cavity of the rib in that zone. The corresponding strain during the first-loading step was thus increased, as shown in Fig. 16a, in which the $\overline{\varepsilon}'_{\text{avg}}$ is the average strain in affected zone. During the second-loading step, M_t is decreased with the initial volume distributed in the first-loading zone increasing (Fig. 16b), and as a result, the strain induced by the transferred material was reduced. Previous research shows that transferred material during the second-loading step is the fundamental reason for strain concentration [11]: the strain during the second-loading step in the affected zone is thus decreased, as shown in Fig. 16a.

Furthermore, Fig. 17a presents the variation rate of the average grain size under different billet volume distributions, and the corresponding variation rate is given as follows:

$$\Delta d(p) = \frac{d(p) - d_{\text{initial}}}{d_{\text{initial}}} \times 100\% \tag{4}$$

where $d(p)$ is the average grain size, $p = 1, 2, 3, 4, 5$; $d_{initial}$ is the initial grain size, which is 10 μm in this work.

It can be seen that three different variation rates are given. The whole variation rate of the first loading step and the second loading step are below the both loading steps. From the perspective of the numerical magnitude, the maximum difference of the variation rate by each single loading step is 7.7% and 4.1% for the first and second loading steps. From grain size distribution in the FE simulation, the grain size

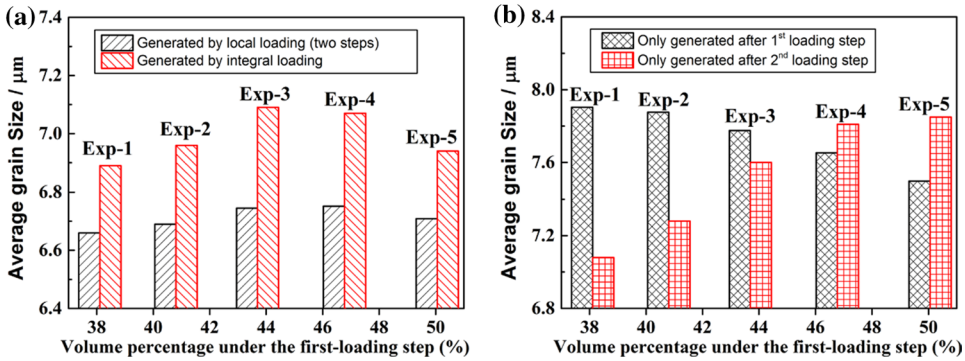

Fig. 15 Influence of the different billet volume distributions on the average grain size of primary equiaxial α: **a** local loading and integral loading; **b** single loading step by local loading

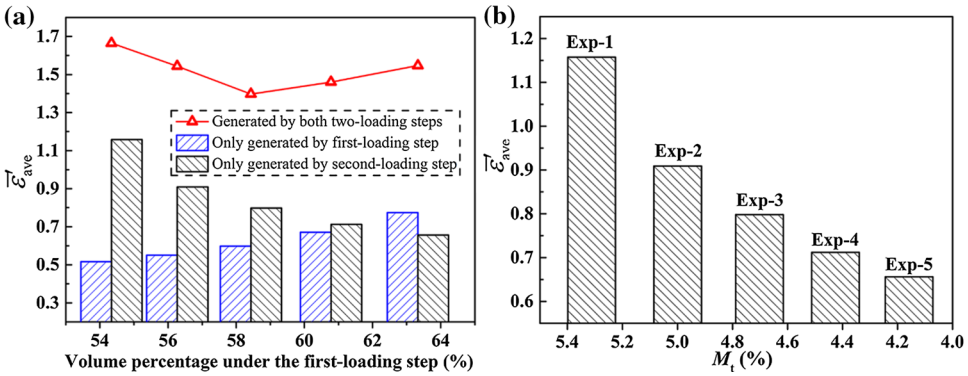

Fig. 16 Influence of the different billet volume distributions on $\overline{\varepsilon}'_{ave}$ [11]: **a** relationship between volume percentage under the first-loading step and $\overline{\varepsilon}'_{ave}$; **b** relationship between M_t and $\overline{\varepsilon}'_{ave}$ during second-loading step

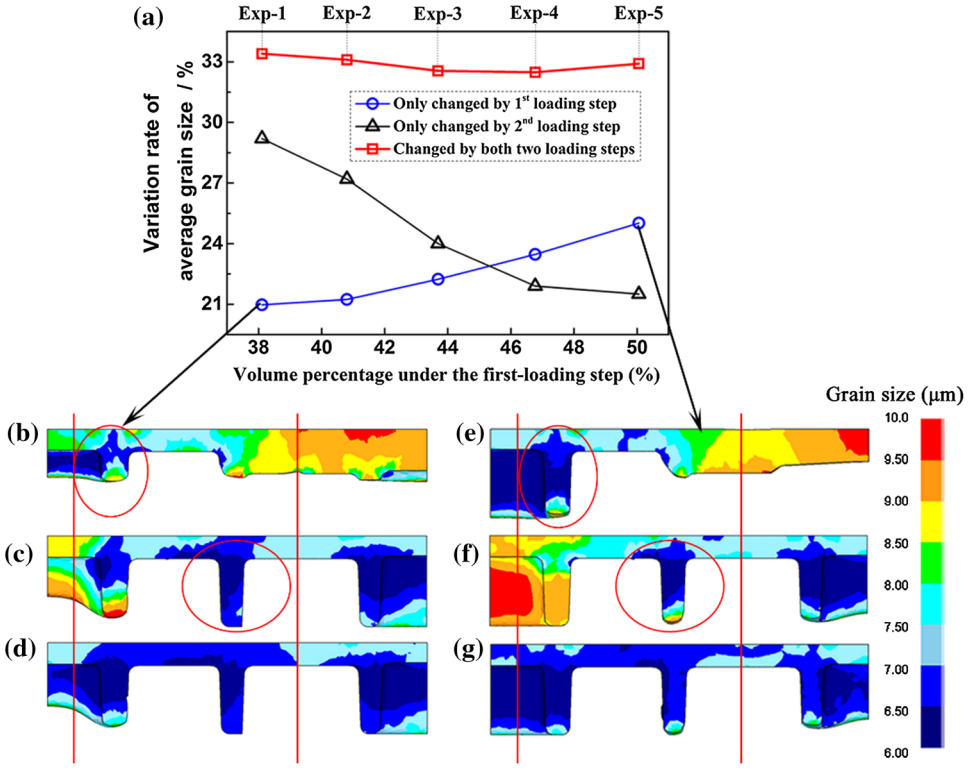

Fig. 17 Influence of the difference billet volume distribution on average grain size and corresponding grain size distribution: **a** variation rate of average grain size; **b**–**g** grain size distribution by first **b**, **e**, single second **c**, **f**, and both **d**, **g** loading steps, respectively

shows a visible difference in Exp-1 and Exp-5, as shown by the symbols with red circle in Fig. 17b, c, e and f. However, that variation rate from both loading steps is less than 1% and the visual of the grain size shows little difference between Exp-1 and Exp-5. Resultantly, the increased initial billet volume of the first-loading zone may have little influence on the average grain size at the end of ILLF.

5 Conclusions

This work focuses on revealing the influence of the billet volume distribution on folding, die underfilling, rib shifting and average grain size of primary equiaxed α in the transitional region of ILLF. The following conclusions were drawn:

(1) The filling depth of the cavity of the rib in the first-loading zone increases with the billet volume of the first-loading increasing, then the transferred material during the second-loading step is decreased accordingly, which is beneficial to reduce the risk of folding and relieve rib shifting.
(2) With the billet volume distribution of the first-loading zone increasing, the die underfilling by two local loading steps decreases first and then increases. Compared with the integral loading and local loading, the variation trend of the die underfilling is the same and the difference on the cavity-filling of the rib is little due to

the reciprocating material transfer during the first and second-loading step.

(3) Comparing with the integral loading, the average grain size is smaller on the whole after the local loading owing to the material transfer and rib shift, which result in strain accumulation during the ILLF process.

(4) With the initial volume in first-loading zone increasing, the average grain size decreases after the first-loading step but increases after the second-loading step. Consequently, the increased initial billet volume of the first-loading zone has little influence on the average grain size at the end of ILLF.

Acknowledgements The authors would like to gratefully acknowledge the support of the Natural Science Foundation of China (Grant No. 52005241), Natural Science Foundation of Jiangxi Province (Grant No. 20192BAB216023), the Key R&D Project in Jiangxi Province of China (Grant No. 20182ABC28001) and PHD Starting Foundation of Nanchang Hangkong University (Grant No. 2030009401056).

References

1. Shen, G., & Furrer, D. (2000). Manufacturing of aerospace forgings. *Journal of Materials Processing Technology, 98*, 189–195.
2. Fan, X. G., Yang, H., & Gao, P. F. (2014). Through-process macro-micro finite element modeling of local loading forming of large-scale complex titanium alloy component for microstructure prediction. *Journal of Materials Processing Technology, 214*(2), 253–266.
3. Kleinera, M., Geigerb, M., & Klaus, A. (2013). Manufacturing of light-weight components by metal forming. *CIRP Annals, 52*(2), 521–542.
4. Yang, H., Wu, C., Li, H. W., et al. (2011). Review on development of key technologies in plastic forming of titanium alloy. *Materials China, 30*(6), 6–13.
5. Yang, H., Fan, X. G., Sun, Z. C., et al. (2011). Some advances in local loading precision forming of large scale integral complex components of titanium alloys. *Materials Research Innovations, 15*(S1), 493–498.
6. Shan, D., Xu, W. C., Si, C. H., et al. (2007). Research on local loading method for an aluminium-alloy hatch with cross ribs and thin webs. *Journal of Materials Processing Technology, 187–188*, 480–485.
7. Sun, Z. C., Yang, H., & Sun, N. G. (2012). Effects of parameters on inhomogeneous deformation and damage in isothermal local loading forming of Ti-Alloy component. *Journal of Materials Engineering and Performance, 21*(3), 313–323.
8. Gao, P. F., Yang, H., & Fan, X. G. (2014). Quantitative analysis of the material flow in transitional region during isothermal local loading forming of Ti-alloy rib-web component. *The International Journal of Advanced Manufacturing Technology, 75*(9), 1339–1347.
9. Gao, P. F., Yang, H., Fan, X. G., et al. (2015). Forming defects control in transitional region during isothermal local loading of Ti-alloy rib-web component. *The International Journal of Advanced Manufacturing Technology, 76*(5), 857–868.
10. Wei, K., Zhan, M., Fan, X. G., et al. (2018). Unequal-thickness billet optimization in transitional region during isothermal local loading forming of Ti-alloy rib-web component using response surface method. *Chinese Journal of Aeronautics, 31*(4), 845–859.
11. Wei, K., Fan, X. G., Zhan, M., et al. (2017). Improving the deformation homogeneity of the transitional region in local loading forming of Ti-alloy rib-web component by optimizing unequal-thickness billet. *The International Journal of Advanced Manufacturing Technology, 92*(9–12), 4017–4029.
12. Fan, X. G., Gao, P. F., & Yang, H. (2011). Microstructure evolution of the transitional region in isothermal local loading of TA15 titanium alloy. *Materials Science and Engineering A, 528*, 2694–2703.
13. Li, Z. Y., Yang, H., & Sun, Z. C. (2008). Research on marco-microcosmic deforming in isothermal local loading transition region for large-scale complex integral components of TA15 titanium alloy. *Rare Metals Materials and Engineering, 37*(9), 1516–1521. (in Chinese).
14. Reza, H. A., & Pouya, Y. (2018). A new criterion for preform design of H-shaped hot die forging based on shape complexity factor. *International Journal of Material Forming, 11*, 233–238.
15. Park, J. J., & Hwang, H. S. (2007). Preform design for precision forging of an asymmetric rib-web type component. *Journal of Materials Processing Technology, 187–188*, 595–599.
16. Sun, Z. C., Yang, H., & Sun, N. G. (2009). Simulation on local loading partition during titanium bulkhead isothermal forming process. *Journal of Plasticity Engineering, 16*(1), 138–143. (in Chinese).
17. Sun, Z. C., & Yang, H. (2009). Analysis on process and forming defects of large-scale complex integral component isothermal local loading. *Materials Science Forum, 614*, 117–122.
18. Hu, C. L., Zeng, F., Zhao, Z., et al. (2015). Process optimization for design of duplex universal joint fork using unequal thickness flash. *International Journal of Precision Engineering and Manufacturing, 16*(12), 2517–2527.
19. Shi, H., Cho, J. R., Yoon, J. W., et al. (2017). Design of thermal stress control layers in the selective deposition technology of hot axle forging dies. *International Journal of Precision Engineering and Manufacturing, 18*(12), 1805–1812.
20. Xiao, H., Fan, X. G., Zhan, M., Liu, B. C., & Zhang, Z. Q. (2020). Flow stress correction for hot compression of titanium alloys considering temperature gradient induced heterogeneous deformation. *Journal of Materials Processing Technology, 2021*(288), 116868.
21. Chen, F., Cui, Z. S., & Chen, J. (2014). Prediction of microstructural evolution during hot forging. *Manufacturing Review, 1*(6), 1–21.
22. Gao, P. F., Yang, H., Fan, X. G., et al. (2015). Quick prediction of the folding defect in transitional region during isothermal local loading forming of titanium alloy large-scale rib-web component based on folding index. *Journal of Materials Processing Technology, 219*, 101–111.
23. Zhang, D. W., & Yang, H. (2013). Numerical study of the friction effects on the metal flow under local loading way. *The International Journal of Advanced Manufacturing Technology, 68*(5–8), 1339–1350.
24. Shen C. W. (2007) Research on material constitution models of TA15 and TC11 titanium alloys in hot deformation processes. *Master Thesis, Northwestern Polytechnical University* (in Chinese)
25. Tang, X. F., Wang, B. Y., Zhang, H., et al. (2017). Study on the microstructure evolution during radial-axial ring rolling of IN718 using a unified internal state variable material model. *International Journal of Mechanical Sciences, 128–129*, 235–252.
26. Han, G. J., Yang, H., Sun, Z. C., et al. (2009). Numerical simulation of microstructure evolution of TA15 alloy large-scale rib-web parts during isothermal local loading process. *Journal of Plasticity Engineering, 16*(5), 112–117. (in Chinese).

27. Robinson, T., Ou, H., & Armstrong, C. G. (2004). Study on ring compression test using physical modeling and FE simulation. *Journal of Materials Processing Technology, 153–154*, 54–59.
28. Dutta, A., & Rao, A. V. (1997). Simulation of isothermal forging of compressor disc by combined numerical and physical modeling techniques. *Journal of Materials Processing Technology, 72*(3), 392–395.
29. Zhang, D. W., Yang, H., Sun, Z. C., et al. (2012). Deformation behavior of variable-thickness region of billet in rib-web component isothermal local loading process. *The International Journal of Advanced Manufacturing Technology, 63*(1–4), 1–12.

Ke Wei received his Ph.D. degree in School of Materials Science and Engineering from Northwestern Polytechnical University. He is a lecturer in Aeronautical Manufacturing Engineering College of NanChang Hangkong University. The main interests of his research include precise plastic forming of light metal alloy for the aerospace applications.

Qing Ma a graduate student of Aeronautical Manufacturing Engineering College of NanChang Hangkong University. His main research interests are the forging simulation and microstructure analysis of the Titanium alloy.

Haibing Tang a graduate student of Aeronautical Manufacturing Engineering College of NanChang Hangkong University. His main research interests are the forging simulation and process optimization for the complex component.

Xiaoguang Fan Professor of Northwestern Polytechnical University, Dean of Material forming and control. The main interests of his research include mechanism and regulation of microstructure evolution in the precise plastic forming of light metal alloy.

Jiang Zhang a Ph.D. candidate in School of Materials Science and Engineering from Northwestern Polytechnical University. His main academic interests are focused on metal forming related with microstructure modeling and FE simulation.